Available online at www.sciencedirect.com
ScienceDirect
Solar Energy 81 (2007) 62–75
SOLAR ENERGY
www.elsevier.com/locate/solener

Mathematical modeling and thermal performance analysis of unglazed transpired solar collectors

M. Augustus Leon, S. Kumar *

Energy Field of Study, Asian Institute of Technology, P.O. Box 4, Klong Luang, Pathumthani 12120, Thailand

Received 21 June 2005; received in revised form 7 March 2006; accepted 14 June 2006
Available online 1 September 2006

Communicated by: Associate Editor Charles Kutscher

Abstract

Unglazed transpired collectors or UTC (also known as perforated collectors) are a relatively new development in solar collector technology, introduced in the early nineties for ventilation air heating. These collectors are used in several large buildings in Canada, USA and Europe, effecting considerable savings in energy and heating costs. Transpired collectors are a potential replacement for glazed flat plate collectors. This paper presents the details of a mathematical model for UTC using heat transfer expressions for the collector components, and empirical relations for estimating the various heat transfer coefficients. It predicts the thermal performance of unglazed transpired solar collectors over a wide range of design and operating conditions. Results of the model were analysed to predict the effects of key parameters on the performance of a UTC for a delivery air temperature of 45–55 °C for drying applications. The parametric studies were carried out by varying the porosity, airflow rate, solar radiation, and solar absorptivity/thermal emissivity, and finding their influence on collector efficiency, heat exchange effectiveness, air temperature rise and useful heat delivered. Results indicate promising thermal performance of UTC in this temperature band, offering itself as an attractive alternate to glazed solar collectors for drying of food products.

The results of the model have been used to develop nomograms, which can be a valuable tool for a collector designer in optimising the design and thermal performance of UTC. It also enables the prediction of the absolute thermal performance of a UTC under a given set of conditions.

1. Introduction

Drying of fruits and vegetables require hot air in the temperature range of 45–60 °C. With abundant solar radiation in the tropical climates of Asia, an unglazed transpired solar collector (UTC) system could readily provide hot air at this temperature range for almost 300 days of the year. Large roof-mounted installations could offer a cost-effective alternative to the expensive glazed collectors to supply significant quantities of hot air for drying applications. A number of ventilation air heating systems based on UTC collectors have been installed in Canada, USA and Europe. As of 2003, more than 80 UTC systems covering a collector area of more than 35,000 m^2 have been installed around the world, mostly for preheating ventilation air. Several UTC-based drying systems have also been installed recently, for drying fruits, nuts, coffee beans, wood chips and barks, wool, and chicken manure (SOLARWALL, 2001/2006). A list of UTC installations used for drying applications is given in Table 1, to highlight the range of size, location and application.

The unglazed transpired solar collector has a dark, perforated vertical/inclined sheet metal absorber is fixed to another parallel surface or wall, with a gap of 10–15 cm between them, with all sides closed and sealed. Ambient

* Corresponding author. Tel.: +66 2 524 5410; fax: +66 2 524 5439.
E-mail address: kumar@ait.ac.th (S. Kumar).

0038-092X/$ - see front matter © 2006 Elsevier Ltd. All rights reserved.
doi:10.1016/j.solener.2006.06.017

Nomenclature

A_s	collector area (m^2)
$C_{p.air}$	specific heat capacity of air (J/kg K)
$C_{p.bp}$	specific heat capacity of back plate material (J/kg K)
$C_{p.col}$	specific heat capacity of absorber material (J/kg K)
D	perforation diameter (m)
d_{plen}	plenum depth (m)
F_{cs}	collector – sky view factor
F_{cg}	collector – ground view factor
F_{cl}	cloud factor
H	absorber height (m)
h	cloud base height (km)
h_{conv}	convective heat transfer coefficient (W/m^2 K)
I_T	solar radiation incident on the collector (W/m^2)
K_{air}	thermal conductivity of air (W/m K)
$m_{air.out}$	mass flow rate of air through the collector (kg/s)
m_{bp}	mass of back plate (kg)
m_{col}	mass of absorber plate (kg)
n_{sky}	fractional area of sky covered by clouds
Nu	Nusselt number
P	pitch of perforations (m)
P_{atm}	atmospheric pressure at the collector location (mbar)
$Q_{conv.air\sim bp}$	convection heat transfer from air to back plate (W)
$Q_{conv.bp\sim amb}$	convection heat transfer from back plate to surrounding air (W)
$Q_{conv.col\sim air}$	convection heat transfer from absorber to air (W)
$Q_{rad.col\sim bp}$	radiation heat transfer from absorber to back plate (W)
$Q_{rad.col\text{-}sur}$	radiation heat transfer from absorber to ambient (W)
$Q_{rad.bp\text{-}sur}$	radiation heat transfer from back plate to surrounding (W)
Re	Reynolds number
T_{amb}	ambient air temperature (K)
$T_{air.out}$	exit air temperature (K)
T_{bp}	temperature of back plate (K)
T_{dp}	dew point temperature (K)
T_{col}	average absorber plate temperature (K)
T_{sky}	sky temperature (K)
T_{sur}	temperature of the surrounding (K)
t	hour of the day (1–24)
v_{app}	approach velocity (m/s)
v_{plen}	plenum air velocity (m/s)
v_{wind}	free stream wind velocity over the absorber and back plate (m/s)
W	absorber width (m)

Greek symbols

α_{col}	solar absorptance of the collector surface
β	absorber porosity
ΔP	total pressure drop across the collector (Pa)
ΔP_{abs}	pressure drop across the absorber plate (Pa)
ΔP_{fric}	frictional pressure drop in the plenum (Pa)
ΔP_{buoy}	buoyancy pressure drop in the plenum (Pa)
ΔP_{acc}	acceleration pressure drop in the plenum (Pa)
ε_{bp}	thermal emissivity of back plate outer surface
ε_{col}	thermal emissivity of the absorber surface facing the sky/ground
$\varepsilon_{col.in}$	thermal emissivity of the absorber surface facing the back plate
ε_{csky}	clear sky emissivity
ε_{hc}	hemispherical cloud emissivity
ε_{HX}	heat exchange effectiveness
ε_{sky}	sky emissivity at collector location
ν	kinematic viscosity (m^2/s)
ρ_{air}	density of air (kg/m^3)
ρ_{col}	density of absorber material (kg/m^3)
ρ_{bp}	density of back plate material (kg/m^3)
μ_{air}	viscosity of ambient air (kg/m s)
η_{col}	collector efficiency

air, pulled through the perforations using a blower, absorbs the heat available at the absorber, and delivers hot air at the blower outlet. These collectors reportedly offer the lowest cost and highest efficiency (60–75%) for air heating (IEA, 1999; Christensen, 1998).

The geometry of the UTC absorber and the operating conditions influence the thermal performance of unglazed transpired solar collectors. Providing transpiration in a UTC serves to enhance the convective heat transfer coefficient between the absorber and the air stream. The suction captures the boundary layer, and significantly reduces wind heat losses; The design allows for elimination of the glazing with its associated cost and optical reflectance.

Studies on UTC to investigate the heat and mass transfer, efficiency, airflow distribution and pressure drop have been carried out since 1991. These include theoretical and empirical models to predict its thermal performance over a wide range of operating conditions. The basic heat loss theory for unglazed transpired collector is explained in detail by Kutscher et al. (1993) and Hollands (1998). Cao et al. (1993) and Golneshan and Hollands (1998), based on experimental results, reported correlations for heat exchange effectiveness for a plate with an array of slits as perforations, with wind flow transverse to the slits. An empirical model for thin plates with circular holes on a triangular layout has been presented by Kutscher (1994), with the wind parallel to the plate. Kutscher (1994) and Van Decker et al. (1996) measured heat exchange effectiveness on thin and thick plates with circular holes on a square or triangular layout over a range of parameters,

Table 1
UTC-based air heating system installations for drying applications

Location/year of installation	Collector size (m^2)	Delivery air temperature/flow rate	Product
Korina Farms, California, USA/2003	465	27 °C/n.a.[a]	Pecan nuts
Xin Zheng Feng Li Food Co.,/China, 2003	56	n.a.	Jujube fruit
Coopeldos R.L., Costa Rica/2003	860	n.a.	Coffee bean
Carriere & Sons, California/2003	300	43 °C/142 $m^3/h\ m^2$	Walnut
Sunsweet Dryers, California, USA/2002	110	n.a./182 $m^3/h\ m^2$	Prune
Kreher's Poultry Farms Clarence, New York, USA/2002	50	n.a./146 $m^3/h\ m^2$	Chicken manure
Hoyt Farm, Casleton, New York, USA/2002	130	n.a.	Wool
Cafe Duran, Panama/2002	900	n.a.	Coffee bean
Biowarme Klein St. Paul Power Plant, Austria/2001	100	60 °C/72 $m^3/h\ m^2$	Shredded wood and bark
Gelee Chicken Farm, Cookshire, Quebec, Canada/2001	158	n.a.	Chicken manure
Malabar, Indonesia/1999	600	35 °C/125 $m^3/h\ m^2$	Tea
Synthite Industrial Chemical Ltd., Coimbatore, India/1998	1300	70 °C	Marigold flowers
ASEAN-Canada Project on Solar Energy, Malaysia/1994	370	60 °C/n.a.	Cocoa
Caribbean/1999	90, 170, 140 (three collectors)	n.a./133, 44, and 55 $m^3/h\ m^2$	Tobacco

Source: SOLARWALL (2001/2006); GPEKS (2006); IEA (1999); Hollick (1999).
[a] Not available.

and presented a correlation for heat exchange effectiveness by fitting the measured data. They also correlated their results with equations involving dimensionless groups such as Reynolds number, ratio of approach velocity to wind velocity, and hole pitch to diameter ratio. Arulanandam et al. (1999) obtained a correlation for heat exchange effectiveness using a CFD model for a plate with circular holes on a square layout, under no-wind conditions. Van Decker et al. (2001) investigated thick and thin plates with circular holes on a square or triangular layout over a range of approach velocities and wind speeds, and presented a relationship for heat exchange effectiveness. Unglazed transpired solar collectors have found most of their applications in ventilation air heating in the high-latitude countries of Northern America and Europe. The studies conducted so far on UTC have mainly concentrated on its performance in such operating conditions, and very few studies have been carried out in tropical weather conditions where the solar input and ambient air temperatures are generally higher, while its use for ventilation air heating is limited. Also, the application of UTC for drying, which means operating the collector for higher delivery air temperatures, has not been studied in detail.

Considering the potential for unglazed transpired solar collectors for drying applications, a mathematical model has been developed for predicting the thermal performance of UTC over a range of design and operating conditions suitable for drying of food products. This article presents the model developed, and an analysis of the performance of the unglazed transpired solar collector. The model predicts the air temperature rise for specific operating conditions, and estimates the UTC design parameters for specific hot air requirements.

2. Development of a mathematical model of unglazed transpired solar collector

2.1. Collector configuration

The configuration of the UTC under analysis is illustrated in Fig. 1. The collector, mounted vertically, has a perforated absorber and a back plate. An air gap separates the absorber sheet from the back plate (known as the plenum). The gaps at the four sides along the absorber edge are closed to form a box. A blower fixed at the top of the box provides the required suction during collector operation.

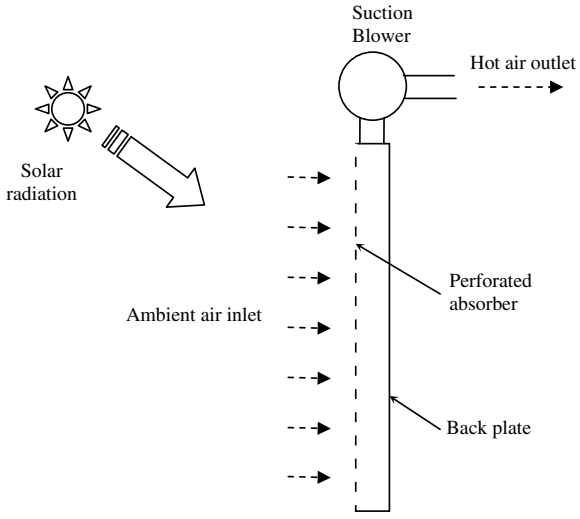

Fig. 1. Schematic of the UTC configuration.

The heat transfer in the unglazed transpired solar collector is studied by considering the overall energy balance between the components of the transpired collector. Rate equations have been used to estimate the convective and radiative heat transfer rates between the components. The model incorporates several empirical relations to calculate the various heat transfer coefficients used in the rate equations.

2.2. Assumptions

The assumptions used in developing the model are listed below:

(i) The absorber and back plate temperatures are assumed to be uniform throughout their respective surfaces (isothermal). While metal absorbers are mostly isothermal from hole-to-hole, non-metal absorbers show some non-isothermality. However, studies by Gawlik (1995), Gawlik and Kutscher (2002) and Gawlik et al., 2005) have shown that the non-isothermality does not have a major impact on collector performance.

(ii) Airflow through the perforations is assumed homogeneous. In reality, due to buoyant flow (driven by the absorbed solar energy, especially in collectors with large height) and friction (due to forced flow) in the plenum, airflow profile could be slightly non-homogeneous, depending on whether the buoyant flow or forced flow dominates (Gunnewiek et al., 1996; Dymond and Kutscher, 1997).

(iii) Convection losses from the absorber plate to the ambient air are considered negligible. In large area collectors, providing a minimum pressure drop of 25 Pa has been shown to reduce absorber convection losses to insignificant levels (Kutscher, 1994).

(iv) Flow reversal through the absorber is assumed to be negligible. Flow reversal is a phenomenon driven by buoyancy and wind, when airflow at the top of the absorber is out of the collector rather than into it. This can however be minimized by providing a minimum pressure drop of 25 Pa across the absorber plate (Kutscher, 1994, 1997; Kutscher et al., 2003).

(v) The absorber is considered to be diffuse, (i.e., one without directional characteristics) and gray (i.e., one independent of wavelength) for all absorbed and emitted radiation.

(vi) Losses along the plenum edge are generally not significant in large area collectors (Summers David, 1996), and hence are neglected.

(vii) An absorber configuration with circular perforations in triangular pitch is assumed. Studies by Kutscher (1994) and Van Decker et al., 1996) have assumed similar absorber configuration.

These assumptions are consistent with studies conducted earlier.

2.3. Energy balance equations

For the present analysis, the energy balance equations for the three collector components—absorber plate, air and the back plate—have been written by considering the solar input, the heat and mass flow rates across the collector, and thermal losses.

The heat transfer modes and heat transfer exchanges in the collector are presented in Fig. 2. The energy input to the system is from the solar radiation received on the absorber surface. The net losses from the system are due to convection and radiation losses from the absorber surface and back plate.

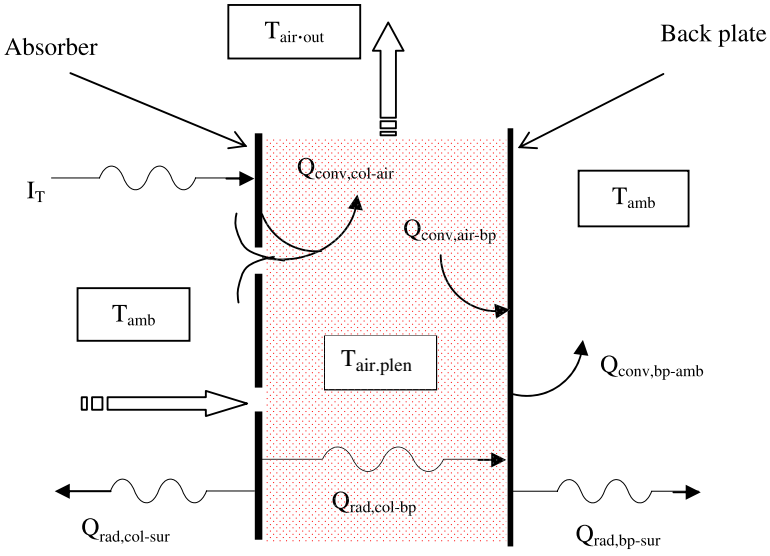

Fig. 2. Heat transfer exchanges in the Unglazed Transpired Solar Collector.

2.3.1. Absorber plate

$$m_{\mathrm{col}} * C_{p.\mathrm{col}} * (\mathrm{d}T_{\mathrm{p}}/\mathrm{d}t) = (\alpha_{\mathrm{col}} * I_{\mathrm{T}} * A_{\mathrm{s}}) - (Q_{\mathrm{conv.col\sim air}} + Q_{\mathrm{rad.col\sim bp}} + Q_{\mathrm{rad.col\sim sur}}) \quad (1)$$

The term $Q_{\mathrm{conv.col\sim air}}$ refers to the heat gain from the absorber plate to air, which includes heat transfer from the absorber front surface, hole and the back surface to the plenum air. $Q_{\mathrm{rad.col\sim bp}}$ gives the radiative heat transfer from the absorber to the back plate. $Q_{\mathrm{rad.col\sim sur}}$ is the term representing the radiative heat loss from the absorber surface to the surrounding.

2.3.2. Plenum air

$$(m_{\mathrm{air.out}} * \mathrm{d}t) * C_{p.\mathrm{air}} * (\mathrm{d}T_{\mathrm{air.out}}/\mathrm{d}t) = Q_{\mathrm{conv.col\sim air}} - Q_{\mathrm{conv.air\sim bp}} \quad (2)$$

$Q_{\mathrm{conv.air\sim bp}}$ in Eq. (2) represents the heat exchange between the back plate and air flowing through the collector.

2.3.3. Back plate

$$m_{\mathrm{bp}} * C_{p.\mathrm{bp}} * (\mathrm{d}T_{\mathrm{bp}}/\mathrm{d}t) = Q_{\mathrm{conv.air\sim bp}} + Q_{\mathrm{rad.col\sim bp}} - Q_{\mathrm{conv.bp\sim amb}} - Q_{\mathrm{rad.bp\sim sur}} \quad (3)$$

While estimating the radiation loss from the back plate to the surrounding, the temperature of the surrounding T_{sur} is calculated from the sky temperature and ground surface temperature.

2.4. Rate equations

2.4.1. Convection heat transfer

The heat transfer rates due to convection were estimated using the convection heat transfer coefficient, the heat transfer surface area, and the temperature difference between the surface and the surrounding fluid. The following correlations were used to estimate the average convection heat transfer coefficients. An average value has been used for the plenum velocity since the velocity varies from zero at the bottom to maximum at the top (Summers David, 1996).

2.4.1.1. Absorber plate to plenum air. Information on convection heat transfer with suction from a hot perforated flat plate is rather limited (Kutscher et al., 1993). The empirical correlation reported by Kutscher (1994) is used in the present model to estimate the Nusselt number.

$$Nu_1 = 2.75 * [(P/D)^{-1.21} * Re_1^{0.43} + 0.011 * \beta * Re_1 * (v_{\mathrm{wind}}/v_{\mathrm{app}})^{0.48}] \quad (4)$$

where

$$Re_1 = (\rho_{\mathrm{air}} * v_{\mathrm{hole}} * D)/\mu_{\mathrm{air}} \quad (5)$$

The convection heat transfer coefficient between the absorber plate and plenum air is then given by

$$h_{\mathrm{conv.col\sim air}} = (Nu_1 * K_{\mathrm{air}})/D \quad (6)$$

Now, $Q_{\mathrm{conv.col\sim air}} = h_{\mathrm{conv.col\sim air}} * (T_{\mathrm{col}} - T_{\mathrm{air.plen}})$.

2.4.1.2. Plenum air to back plate. The Nusselt number for convection heat transfer between the plenum air and back plate,

$$Nu_2 = 0.664 * (Re_2)^{0.5} * (Pr_2)^{0.333} \quad (7)$$

where

$$Re_2 = (\rho_{\mathrm{air}} * v_{\mathrm{plen}} * H)/\mu_{\mathrm{air}} \quad (8)$$

$$Pr_2 = (C_{p.\mathrm{air}} * \mu_{\mathrm{air}})/K_{\mathrm{air}} \quad (9)$$

Convective heat transfer coefficient between the air and the back plate is estimated from

$$h_{\mathrm{conv.air\sim bp}} = (Nu_2 * K_{\mathrm{air}})/d_{\mathrm{plen}} \quad (10)$$

The convection heat transfer between the plenum air and back plate

$$Q_{\mathrm{conv.air\sim bp}} = h_{\mathrm{conv.air\sim bp}} * (T_{\mathrm{air.plen}} - T_{\mathrm{bp}}) \quad (11)$$

2.4.1.3. Absorber plate to ambient. Convection heat losses from the absorber surface of an UTC to the ambient air are negligible during its normal operation as the convective boundary layer is continuously sucked off (Kutscher, 1992, 1994; Arulanandam et al., 1999). Providing a minimum pressure drop of 25 Pa and a minimum approach velocity (estimated as the flow rate per unit area of collector at which outside air is drawn into the collector) of 0.02 m/s has been shown to reduce absorber convection losses to insignificant levels in large area collectors (Kutscher, 1994; Summers David, 1996). As the present analysis considers 25 Pa and 0.02 m/s as the lower limits for absorber pressure drop and approach velocity respectively, the convective heat loss component has been neglected.

2.4.1.4. Back plate to ambient. The Nusselt number in the above expression is calculated using the following correlation (Cengel and Turner, 2001):

$$Nu_3 = 0.664 * (Re_3)^{0.5} * (Pr_3)^{0.333} \quad (12)$$

$$Re_3 = (\rho_{\mathrm{air}} * v_{\mathrm{wind}} * W)/\mu_{\mathrm{air}} \quad (13)$$

Convection heat transfer coefficient:

$$h_{\mathrm{conv.bp\sim amb}} = (Nu_3 * K_{\mathrm{air}})/L_{\mathrm{c}} \quad (14)$$

$$\text{Now, } Q_{\mathrm{conv.bp\sim amb}} = h_{\mathrm{conv.bp\sim amb}} * (T_{\mathrm{bp}} - T_{\mathrm{amb}}) \quad (15)$$

2.4.2. Radiation heat transfer

The heat transfer rates due to radiation were estimated using the Stefan–Boltzmann law, involving the total radiating area, absolute temperature of the radiating body, and Stefan–Boltzmann constant.

2.4.2.1. Absorber plate to ambient. Radiation heat loss from the absorber surface occurs both to the sky and to the ground, with the view factor depending on the absorber tilt. Noting that the absorber has been considered as gray and diffuse, the radiation heat loss from the absorber is

$$Q_{\text{rad.col}\sim\text{sur}} = \varepsilon_{\text{col}} * \sigma_{\text{sb}} * A_{\text{s}} * (T_{\text{col}}^4 - F_{\text{cs}} T_{\text{sky}}^4 - F_{\text{cg}} T_{\text{gnd}}^4) \quad (16)$$

Several correlations are available for the estimation of sky temperature T_{sky} (Bliss, 1961; Swinbank, 1963; Berger et al., 1984; Martin and Berdahl, 1984). In the present study, a sub-routine based on the correlation developed by Martin and Berdhal has been used.

$$T_{\text{sky}} = \varepsilon_{\text{sky}}^{0.25} * T_{\text{amb}} \quad (17)$$

where sky emissivity

$$\varepsilon_{\text{sky}} = \varepsilon_{\text{csky}} + (1 - \varepsilon_{\text{csky}}) * n_{\text{sky}} * \varepsilon_{\text{hc}} * F_{\text{cl}} \quad (18)$$

and the clear sky emissivity

$$\varepsilon_{\text{csky}} = 0.711 + 0.56\left(\frac{T_{\text{dp}}}{100}\right) + 0.73\left(\frac{T_{\text{dp}}}{100}\right)^2 + 0.013\cos\left[\frac{\pi t}{12}\right] + 0.00012(P_{\text{atm}} - 1000) \quad (19)$$

where t is the hour of the day. The cloud factor F_{cl} is computed by the sub-routine internally from the solar radiation data.

The ground surface temperature T_{gnd} depends on several factors such as the surface exposure to insolation, wind speed, soil moisture, vegetation cover and vegetation height, and its determination is complex (Signorelli and Kohl, 2004). Considering that the ground surface temperature variation coincides with the local air temperature variation (Bi et al., 2004), and that the the daily mean surface temperature is commonly near the mean air temperature (GSFC, 2006), T_{gnd} has been taken as the ambient air temperature T_{amb}.

Radiative heat transfer rates from absorber plate to back plate, and from back plate to the surroundings were estimated using the temperature and emissivity values of the collector components.

2.4.2.2. Absorber plate to back plate. The radiation heat transfer between the absorber plate and back plate was estimated using the following relation:

$$Q_{\text{rad.col}\sim\text{bp}} = \sigma_{\text{sb}} * A_{\text{s}} * (T_{\text{col}}^4 - T_{\text{bp}}^4)/(1/\varepsilon_{\text{col.in}} + 1/\varepsilon_{\text{bp}} - 1) \quad (20)$$

The emissivity of the inner surface of the absorber is taken to be different from that of the outer surface since the outer surface generally has a coating of high absorptivity. The inner surface of the absorber is normally bare, free of any coating.

2.4.2.3. Back plate to surrounding. The radiation heat transfer from the back plate to the surrounding was estimated using the following relation:

$$Q_{\text{rad.bp}\sim\text{sur}} = \varepsilon_{\text{bp}} * \sigma_{\text{sb}} * A_{\text{s}} * (T_{\text{bp}}^4 - T_{\text{sur}}^4) \quad (21)$$

The emissivity of both the surfaces of the back plate are assumed to be equal.

2.5. Collector efficiency

The efficiency of the unglazed transpired solar collector is the ratio of the useful heat delivered by the solar collector to the total solar energy input on the collector surface. The useful heat delivered by the collector can be estimated from the temperature and flow rate of the outlet air. Therefore,

$$\eta_{\text{col}} = \frac{m_{\text{air.out}} C_{\text{p.air}} (T_{\text{air.out}} - T_{\text{amp}})}{I_{\text{T}} A_{\text{s}}} \quad (22)$$

2.6. Heat exchange effectiveness

Heat exchange effectiveness of an UTC depends on the overall heat transfer coefficient for the air passing through the absorber, and is defined as the ratio of the actual temperature rise of air as it passes through the absorber plate to the maximum possible temperature rise (Kutscher, 1994). Mathematically,

$$\varepsilon_{\text{HX}} = \frac{T_{\text{air.plen}} - T_{\text{amb}}}{T_{\text{col}} - T_{\text{amb}}} \quad (23)$$

Heat exchange effectiveness ε_{HX} between the absorber and plenum air can be estimated using the relationship based on logarithmic mean temperature difference (LMTD) applied for heat exchangers (Kutscher, 1992, 1994).

$$\varepsilon_{\text{HX}} = 1 - \exp[-h_{\text{conv.col}\sim\text{air}} * A_{\text{s}}/(m_{\text{air.out}} * C_{p.\text{air}})] \quad (24)$$

These two expressions provide a relation between the exit air temperature, absorber temperature and ambient temperature.

2.7. Pressure drop

Total pressure drop across the collector (ΔP) is a sum of pressure drop across the absorber plate (ΔP_{abs}), and pressure drops in the plenum, which include frictional pressure drop (ΔP_{fric}), buoyancy pressure drop (ΔP_{buoy}) and acceleration pressure drop (ΔP_{acc}) (Kutscher, 1994; Dymond and Kutscher, 1997).

$$\text{i.e.,}\quad \Delta P = \Delta P_{\text{abs}} + \Delta P_{\text{fric}} - \Delta P_{\text{buoy}} + \Delta P_{\text{acc}} \quad (25)$$

Buoyancy force tends to push the plenum air up, acting in the direction opposite to that of frictional force.

Pressure drop across the absorber plate has to be at least 25 Pa to ensure a uniform flow and temperature distribution over the collector (Kutscher, 1997). If temperature distribution is not uniform, hot spots could develop on the collector surface, which will increase the radiation loss to the surroundings (Kokko and Marshal, 1992).

3. Data and solution procedure

The energy balance and rate equations described in Section 2 were solved to find the exit air temperature, heat exchange effectiveness, collector efficiency and heat delivered for a given set of input values, and for a given time period. The intermediate values would include the estimation of the heat transfer coefficients and heat flux between the UTC components. For subsequent times, the initial temperatures are specified equal to the temperature values of the respective previous sections. The iterative process is continued until the end time is reached. As initial condition, the absorber plate, back plate and plenum air are all assumed to be at ambient temperature.

As noted by earlier studies (Kutscher et al., 1993; Kutscher, 1994; Van Decker et al., 1996, 2001), the key parameters of an UTC system include perforation diameter, pitch, airflow rate/approach velocity, collector absorptivity/emissivity, solar radiation, and wind velocity. A parametric analysis was conducted for a range of perforation diameter–pitch combinations, radiation and airflow rates. Triangular pitch was assumed for the absorber perforations. The input parameters considered for the analysis are: (a) porosity (involving perforation diameter and pitch), (b) approach velocity, (c) solar radiation, and (d) solar absorptivity/thermal emissivity.

The range of parameters selected for the present analysis was as below.

(i) *Approach velocity*: For drying of most food products, a drying air temperature of 50–60 °C is required, which can be attained only at low approach velocities. Tests at NREL (National Renewable Energy Laboratory, USA) showed that below the approach velocity of 0.02 m/s, performance is worse than theoretical prediction perhaps because of natural convection effects, or non-homogeneous suction. These flow rates result in high absorber surface temperatures and associated low collector efficiency. Considering this minimum requirement, in the present study, an approach velocity range of 0.02–0.03 m/s was selected, which is equivalent to an airflow rate of 72–108 $m^3/h\ m^2$ of collector area. However, in some cases, the range has been increased to 0.0125–0.0375 m/s.

(ii) *Solar radiation*: A solar radiation range of 400–900 W/m^2 was selected for the analysis, which reasonably corresponds to the daily average solar radiation in tropical locations.

(iii) *Absorber pressure drop*: A minimum absorber pressure drop of 25 Pa is required to ensure uniform flow distribution through the collector. However, a slightly lower pressure drop may be allowable if the approach velocity is maintained above 0.02 m/s (Summers David, 1996). The upper limit to absorber pressure drop is guided by the power consumption by the suction blower, which will become excessive at pressure drops higher than 80 Pa. A pressure drop range of 25–80 Pa was therefore selected for the current study.

(iv) *Collector plenum*: The frictional pressure drop across the collector was estimated using the model over a plenum (distance between the absorber and back plate) range of 50–150 mm. For the selected collector parameters, a plenum of 120 mm was found to be sufficient to keep the frictional pressure drop to a minimum. A higher value may be required for larger airflow rates as in the case of ventilation air heating applications.

(v) *Pitch and perforation diameter*: Considering past studies on the pitch of perforations (Kutscher, 1992, 1994; Van Decker and Hollands, 1999; Arulanandam et al., 1999), a pitch range of 12–24 mm was selected for the present study, which corresponds to a perforation diameter of 0.80–1.55 mm. Lower values of pitch dictate absorbers with very small perforation diameters, and could pose manufacturing difficulties. A perforation diameter of 0.8 mm has been used in commercial collectors. Larger values of pitch tend to lower the collector efficiency and heat exchange effectiveness.

Table 2 summarises the input parameters and the range of their values used in the present study.

The output parameters estimated were (a) collector efficiency, (b) heat exchange effectiveness, (c) air temperature rise (or delivery air temperature), and (d) useful heat delivered. The effect of varying the input parameters on these were also studied.

For the collector with mild steel absorber coated with flat black paint, within the selected range of solar radiation and airflow rate, the UTC simulation was performed for a number of combinations of pitch and perforation diameter. The results are discussed in the following sections.

Table 2
Input parameters and their values used in the study

S. No.	Input parameter	Range
1	Approach velocity	0.02–0.03 m/s
2	Solar radiation	400–900 W/m^2
3	Ambient temperature	30 °C
4	Wind velocity	1.2 m/s
5	Pressure drop across the absorber	25–80 Pa
6	Plenum depth	120 mm
7	Pitch (triangular)	12–24 mm
8	Perforation diameter	0.80–1.55 mm
9	Absorber material	Mild steel
10	Design parameters used for reference collector	
	Solar absorptance	0.95
	Thermal emittance	0.85
	Pitch	20 mm
	Perforation diameter	1.25 mm

4. Simulation results and analysis

To investigate the effect of the seven parameters (pitch, perforation diameter, solar radiation, airflow rate, solar absorptivity and thermal emissivity) on the UTC performance, each parameter was varied, keeping the others constant. The results of this analysis are presented in this section.

4.1. Effect of perforation diameter and pitch on air temperature rise

Perforation diameter and pitch in a UTC affects its performance significantly, especially at low airflow rates and high solar input, typical for drying applications in the tropical climate of Asia. At an airflow rate of 72 $m^3/h\ m^2$ and solar radiation of 900 W/m^2, changing the pitch from 12 to 24 mm (and a corresponding change in perforation diameter from 0.80 to 1.55 mm) results in a drop of 5.5 °C in the air temperature rise. Thus, for a constant airflow rate and solar radiation, air temperature rise increases with decreasing pitch–perforation diameter-flow rate combination.

In the case of UTC, for a constant airflow rate and solar radiation, highest air temperature rise was obtained for the smallest pitch–diameter combination. Hence, smaller pitch–diameter-flow rate combinations are generally preferable for applications that require higher air temperatures such as drying.

Fig. 3 also presents the range of air temperature rise obtained during normal collector operation. At an airflow rate of 72 $m^3/h\ m^2$, the UTC provides an average air temperature rise of 11, 17 and 23 °C for solar radiation levels of 400, 650 and 900 W/m^2 respectively. In comparison, a natural convection type single-glazed solar air collector with corrugated aluminium absorber (and insulation at the back) typically offers an average temperature rise of 25 °C at a solar radiation of 900 W/m^2 (Pangavhane et al., 2002). A double-glazed collector with flat absorber, operated in forced convection mode at a similar airflow rate of 72 $m^3/h\ m^2$ can deliver a temperature rise of about 29 °C at a solar radiation of 915 W/m^2 (Löf, 1981).

4.2. Effect of perforation diameter and pitch on heat exchange effectiveness and efficiency

Fig. 4 presents the collector performance in terms of heat exchange effectiveness for the range of pitch and perforation diameters considered.

For smaller pitch–diameter combination, the heat exchange effectiveness improves from about 0.6 to 0.8. For a particular pitch, any change in perforation diameter affects the heat exchange effectiveness only moderately. For a pitch of 18 mm, a change in diameter from 1.25 to 1.55 mm results only in a 1.4% drop in effectiveness.

Figs. 5 and 6 show the influence of pitch and approach velocity on heat exchange effectiveness and efficiency. For a constant airflow, increasing the pitch decreases the heat exchange effectiveness. An increase in pitch from 12 to 24 mm (for an airflow rate of 72 $m^3/h\ m^2$) results in a 11.5% drop in effectiveness.

Pitch also has an effect on collector efficiency, but the effect is less pronounced. Increasing the pitch from 12 to 24 mm results in a 3% decrease in collector efficiency.

Figs. 5 and 6 indicate that the pitch has a stronger influence on heat exchange effectiveness than on efficiency. With larger pitches, hot spots tend to develop on the absorber surface on locations which are away from and surrounding the perforations (Arulanandam et al., 1999). These, in turn, could increase the radiation heat loss from the absorber, and cause the efficiency to drop.

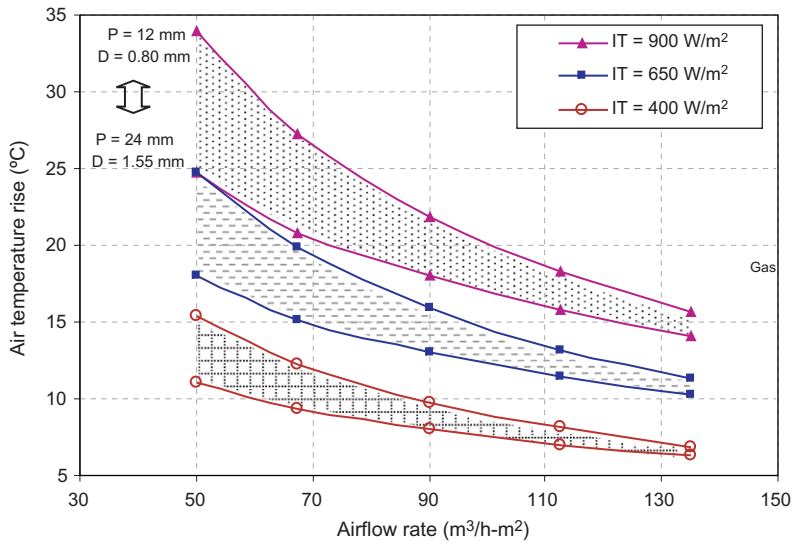

Fig. 3. Air temperature rise for various airflow rates, for an ambient temperature of 30 °C.

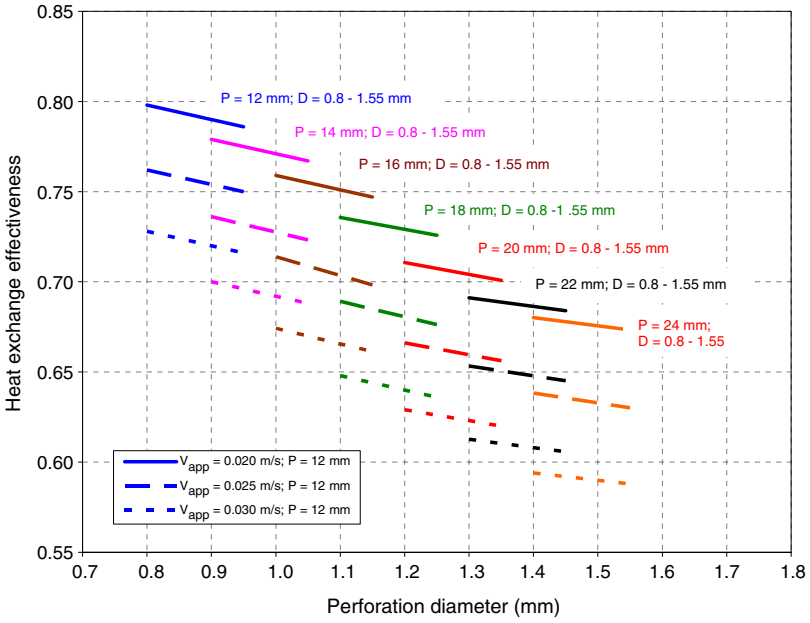

Fig. 4. Heat exchange effectiveness as a function of collector pitch and perforation diameter.

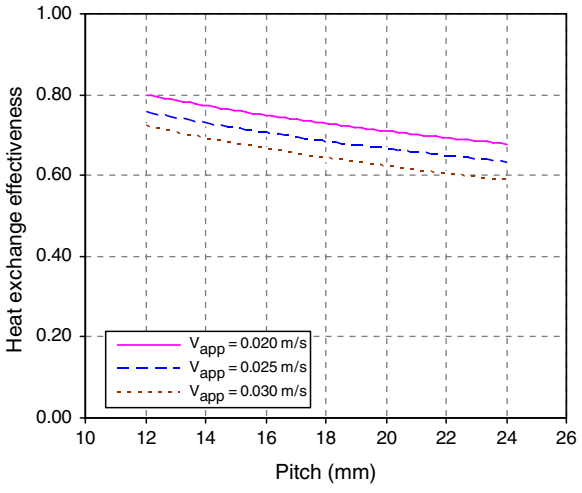

Fig. 5. Heat exchange effectiveness as a function of perforation pitch.

4.3. Effect of absorber porosity on heat exchange effectiveness and efficiency

For constant pitch, increasing the porosity decreases the heat exchange effectiveness, but not significantly. Increasing the porosity from 0.40% to 0.57%, i.e., by 42% (or increasing the perforation diameter from 0.80 to 0.95 mm), results in a 1.2% drop in effectiveness (Fig. 7). However, increasing the pitch decreases the heat exchange effectiveness considerably, as discussed earlier (Section 4.2).

The effect of porosity on collector efficiency is also insignificant. For the same 42% increase in porosity (i.e., from 0.40% to 0.57%), the efficiency drop is less than 2% (Fig. 8). As discussed in Section 4.2, pitch has a lesser influence on collector efficiency than heat exchange effectiveness.

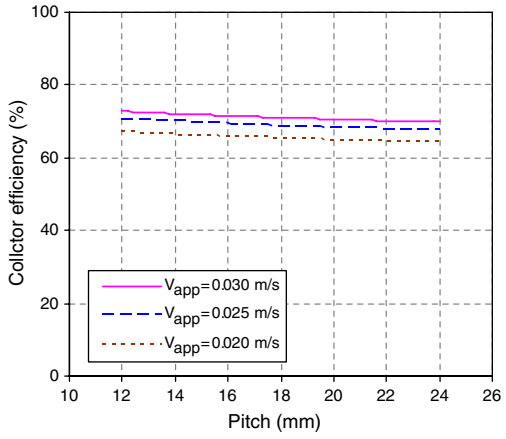

Fig. 6. Collector efficiency as a function of perforation pitch.

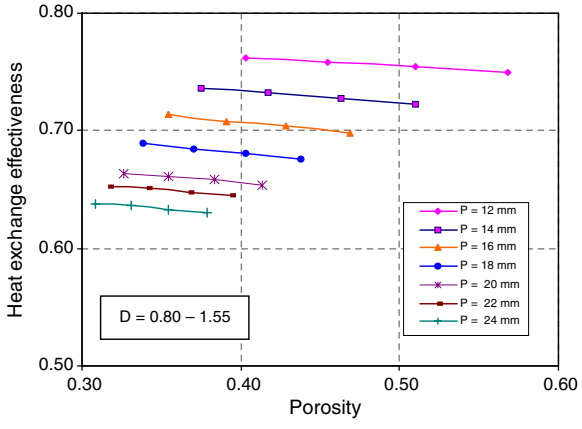

Fig. 7. Effect of absorber porosity on heat exchange effectiveness, for an approach velocity of 0.025 m/s.

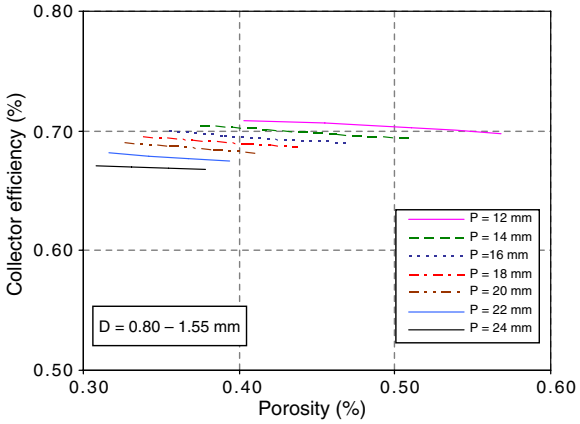

Fig. 8. Effect of absorber porosity on collector efficiency, for an approach velocity of 0.025 m/s.

4.4. Effect of solar radiation and airflow rate on exit air temperature

Fig. 9 presents the simulation results on exit air temperature–airflow rate relationship for different levels of solar radiation for a typical unglazed transpired solar collector. For an ambient temperature of 30 °C, pitch of 20 mm and perforation diameter of 1.25 mm, the results of the simulation studies were compiled for five different airflow rates and plotted in the same graph. Fig. 9 provides the relationship between the key parameters (delivery air temperature, solar radiation and airflow rate), required in designing a UTC system for specific air temperature requirements.

The results indicate slight over-prediction of exit air temperature (or air temperature rise) in comparison with similar plots of SOLARWALL (2001/2006), especially at very low airflow rates. For flow rates above 67.5 $m^3/h\,m^2$, the two graphs show good agreement. For example, the present results predict a temperature rise of 24 °C for an airflow of 72 $m^3/h\,m^2$ at 900 W/m^2 of solar radiation, against 22.5 °C estimated by SOLARWALL. As indicated in the figure, air temperatures in the range of 45–55 °C can be easily achieved by the UTC, which is well suited for drying fruits and vegetables.

Fig. 10 presents the exit air temperature and heat delivered by air flowing through the collector. As with any solar collector, UTC efficiency decreases with increasing delivery air temperatures. However, with collector efficiency in excess of 65% for the given range of airflow rate (Fig. 6), the amount of heat delivered by the UTC is higher than most other conventional glazed and unglazed solar collectors.

The air temperature prediction by the model compares well with the simulation results of Pesaran and Wipke (1994), who have investigated the use of UTC for desiccant cooling. At a solar radiation of 700 W/m^2, for an approach velocity of 0.02 m/s, the present model predicts a delivery air temperature of 49 °C, compared to 48 °C by Pesaran and Wipke.

In Fig. 10, the rate of heat delivery increases at a lower rate at lower approach velocities. This may be due to the increasing losses from the collector at lower approach velocities (or airflow rates), resulting in higher collector operating temperatures.

4.5. Effect of approach velocity on heat exchange effectiveness and collector efficiency

The influence of approach velocity on the UTC's performance was studied. For the given collector parameters, at a constant level of solar radiation, heat exchange effectiveness decreases with increasing approach velocity. Fig. 11

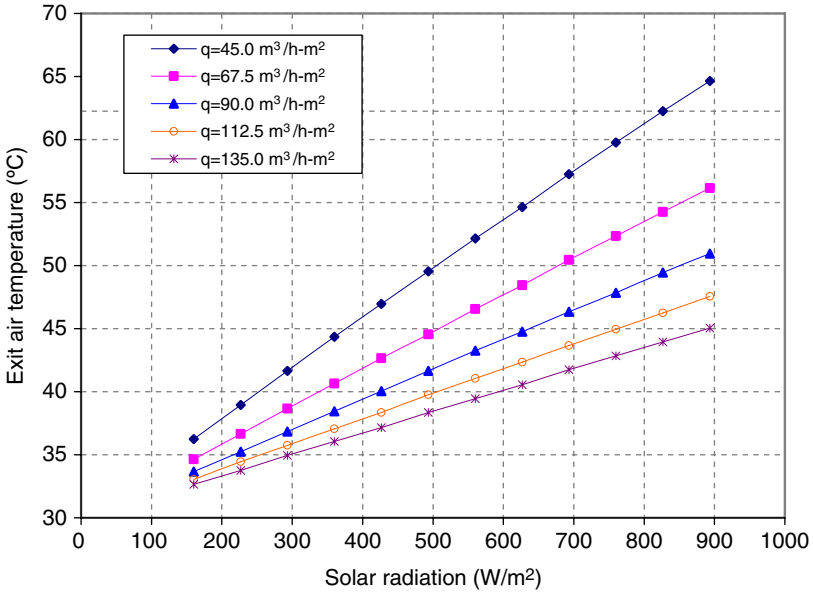

Fig. 9. Exit air temperature as a function of solar radiation and airflow rate.

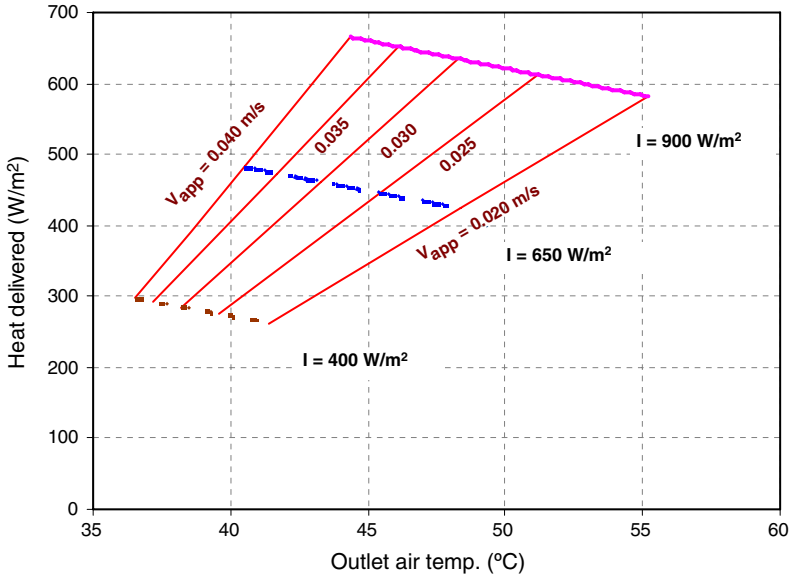

Fig. 10. Delivery air temperature and heat delivered for three radiation levels, for an approach velocity range of 0.02–0.04 m/s.

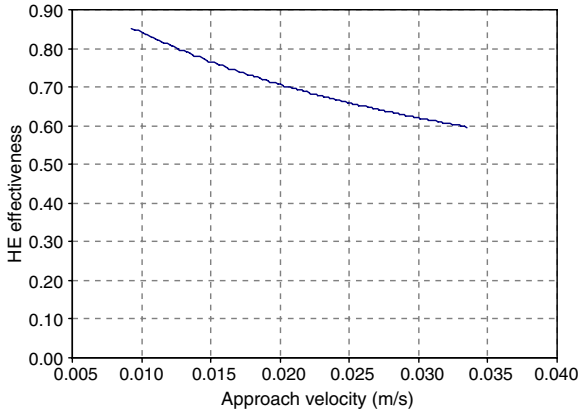

Fig. 11. Effect of approach velocity on collector heat exchange effectiveness.

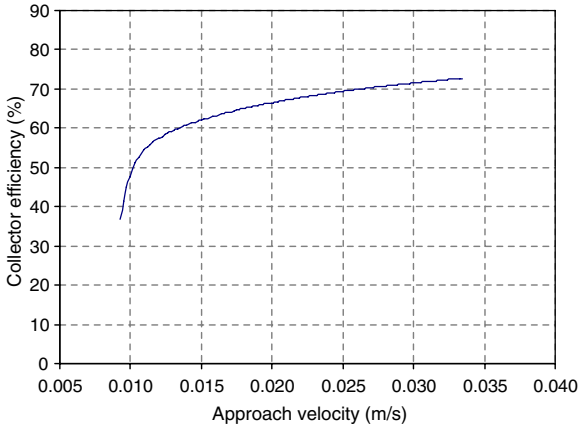

Fig. 12. Effect of approach velocity on collector efficiency.

presents the relationship between approach velocity and heat exchange effectiveness for an absorber with 1.25 mm perforations, at 20 mm square pitch. A change in approach velocity from 0.01 to 0.03 m/s resulted in a corresponding drop in effectiveness of about 23%, indicating the strong influence of approach velocity on heat exchange effectiveness.

Fig. 12 illustrates the effect of approach velocity on collector efficiency for the same collector configuration. Due to the linear relationship between approach velocity and airflow rate, any increase in airflow rate means a proportional increase in approach velocity. As approach velocity is increased, collector efficiency rises, rapidly at low velocities, (between 0.009 and 0.014 m/s), but only slightly at rates above 0.014 m/s. For approach velocities greater than 0.03 m/s, efficiency is nearly constant. The results are generally in consistent with earlier studies. Kutscher et al. (1993) have noted that the efficiency is nearly constant for approach velocities greater than 0.05 m/s.

Increasing the approach velocity enhances the collector efficiency, since higher airflows resulting from higher approach velocities tend to operate the collector at lower temperature levels, which results in lower overall losses from the collector.

4.6. Effect of solar absorptivity and thermal emissivity on collector efficiency

The effects of solar absorptivity and thermal emissivity on collector efficiency are presented in Figs. 13 and 14. At an approach velocity range of 0.02–0.03 m/s, the efficiency reduced by about 35% when absorptivity was reduced from 0.95 to 0.50. For the same range of approach velocity, efficiency reduced by about 12.5% when the emissivity was increased from 0.25 to 0.85. Absorptivity, thus, has a stronger effect on efficiency than the thermal emissivity as absorptivity directly influences the energy input to the collector, and therefore the efficiency. Emissivity how-

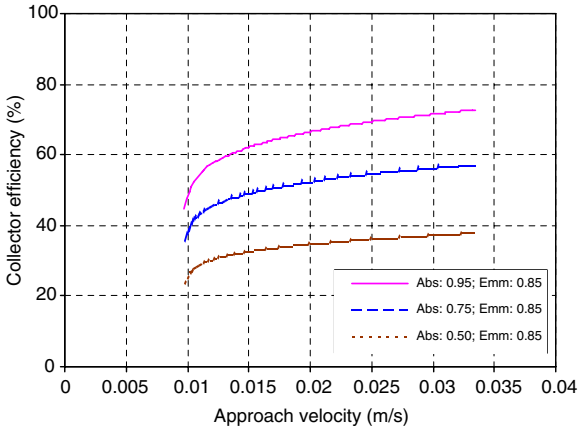

Fig. 13. Effect of solar absorptivity on collector efficiency (ε_{col}: 0.85).

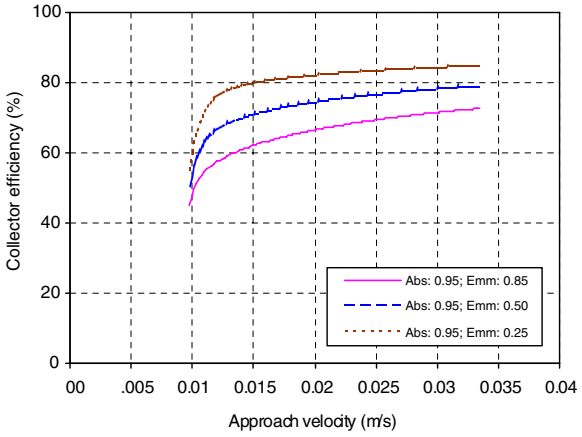

Fig. 14. Effect of thermal emissivity on collector efficiency (α_{col}: 0.95).

ever affects only the radiant heat loss from the collector, and hence its effect on efficiency is relatively less.

Figs. 15 and 16 illustrate the relationship between solar absorptivity, thermal emissivity, delivery air temperature and heat output by the collector. As in Figs. 13 and 14,

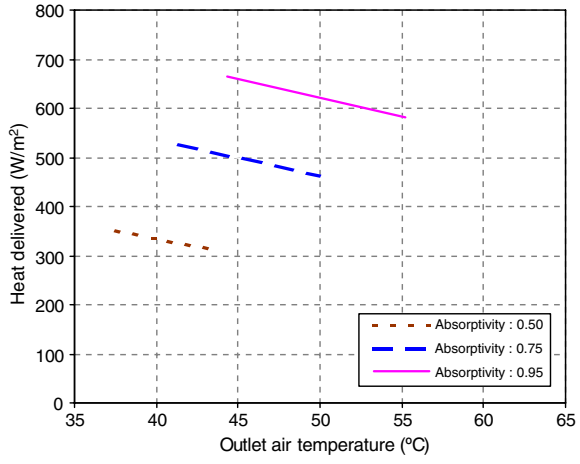

Fig. 15. Effect of solar absorptivity on outlet air temperature and heat delivered (ε_{col}: 0.85; airflow rate: 0.02–0.04 m/s).

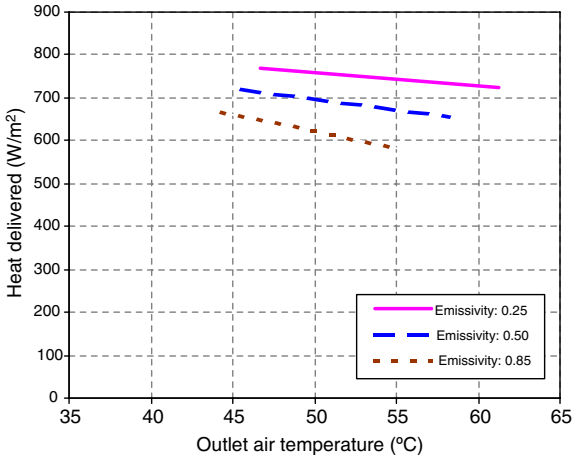

Fig. 16. Effect of thermal emissivity on outlet air temperature and heat delivered (α_{col}: 0.95; airflow rate: 0.02–0.04 m/s).

solar absorptivity has a stronger influence on delivery air temperature and heat output.

The effect of emissivity on the heat output and therefore efficiency is significant at high outlet air temperatures (over 50 °C). Pesaran and Wipke (1994) have observed similar results while investigating a UTC at similar operating conditions. This indicates that emissivity plays a larger role when the collector is operated at higher temperatures.

Table 3 presents a comparison of the model results of this study with simulation results in the literature. Though many results in earlier studies that have the same objectives are comparable, there are additional results from the simulation presented here, especially those related to the influence of perforation diameter and pitch, and the absorber porosity. Some other outputs (Figs. 3–8) could not be compared as similar information is not available in the literature.

5. Nomograms

Figs. 9 and 10 can be used to predict the thermal performance of a UTC system. The nomograms are based on the simulation results for a UTC collector with 20 mm pitch, 1.25 mm perforation diameter, and an absorber coated with flat black paint, and would cater to conditions suitable for drying applications. Using Fig. 9, the average delivery air temperature can be predicted depending on the flow rate required, by a knowledge of the average daily solar radiation. Alternatively, the average flow rate that can be obtained from the collector for a particular delivery air temperature can be estimated for a given solar radiation. Fig. 10 can be used for estimating the heat delivered by the UTC system under specific operating conditions (approach velocity, delivery air temperature and solar radiation). An example demonstrating its application is described below.

A UTC collector (of similar design as the one presented in this study) is to be operated at Bangkok, Thailand, at a

Table 3
Comparison of simulation results from the present study with earlier studies

S. No.	Parametric study	Results	
		Present study	Earlier studies
1	Effect of perforation diameter and pitch	• For a constant airflow rate and solar radiation, air temperature rise increases with decreasing pitch–perforation diameter-flow rate combination • For a constant airflow, heat exchange effectiveness (HEE) and efficiency decrease with increasing pitch; pitch has a stronger influence on HEE than on efficiency • For a particular pitch, any change in perforation diameter affects the heat exchange effectiveness only moderately	• HEE decreases with increasing pitch, perforation diameter and approach velocity (Van Decker and Hollands, 1999)
2	Effect of absorber porosity	• For a constant pitch, increasing the porosity marginally decreases the HEE and collector efficiency	
3	Influence of solar radiation and airflow rate	• Solar radiation levels do not influence collector efficiency significantly • Collector efficiency decreases with increasing delivery air temperatures	• Efficiency can slightly increase or decrease with variations in radiation levels (Kutscher et al., 1991) • Efficiency decreases with increasing delivery air temperatures (Pesaran and Wipke, 1994)
4	Effect of approach velocity	• At constant solar radiation, with increasing approach velocity, collector efficiency increases while HEE decreases • Delivery air temperature and heat delivered decreases with increasing approach velocity. The rate of decrease in heat delivered is lower at lower approach velocities • Collector efficiency rises rapidly between approach velocities of 0.009 and 0.014 m/s, and moderately thereafter. For approach velocities greater than 0.03 m/s, efficiency is nearly constant	• Efficiency increases with increasing approach velocity (Kutscher et al., 1993) • To get high efficiency, the average approach velocity should be small, especially in large area collectors with non-uniform flow, with approach velocity higher at the bottom (Gunnewiek et al., 1996) • For approach velocities greater than 0.05 m/s, efficiencies are nearly constant (Kutscher et al., 1993)
5	Effect of absorptivity and emissivity	• The effect of emissivity on the heat output and therefore efficiency is significantly high at high delivery air temperatures • Solar absorptivity has a stronger effect on efficiency than the thermal emissivity	• At high delivery air temperatures, emissivity has a significant impact on collector performance (Pesaran and Wipke, 1992) • Solar absorptivity has a significantly larger effect than emissivity (IEA, 1999)

solar radiation of 850 W/m^2 to supply hot air at 50 °C. Calculate the optimum airflow rate, heat delivered by the collector, and collector efficiency.

From Fig. 10, the airflow rate and heat delivered corresponding to a solar radiation of 850 W/m^2 and delivery air temperature of 50 °C are obtained as 0.0240 m^3/s m^2 (86.4 m^3/h m^2) and 550 W/m^2 respectively. The collector efficiency is the ratio between the heat delivered and solar input, which, in this case, is 64.7%. If the available solar radiation is 750 W/m^2, hot air can be obtained at a temperature of 50 °C if the flow rate is maintained at 0.0215 m^3/s m^2. If a higher flow rate, is required, a drop in delivery air temperature is to be expected. The nomograms presented here are only applicable to the particular collector specification noted earlier. However, the model may be used to generate similar graphs for any collector design.

6. Conclusion

A model based on heat balance and rate equations for unglazed transpired solar collector (UTC) has been developed to predict its thermal performance over a wide range of design and operating conditions. Results of the model were used to show the effects of key parameters on the performance of a UTC for a delivery air temperature of 45–55 °C, aimed at its use in solar drying applications.

The observations indicate that solar absorptivity, collector pitch, and approach velocity (or airflow rate) have the strongest effect on collector heat exchange effectiveness as well as efficiency. The effect of thermal emissivity and porosity on heat exchange effectiveness seems to be moderate. Results indicate promising thermal performance of UTC in the temperature range of 45–55 °C, offering itself as an attractive alternate to glazed solar collectors for drying of food products. However, establishing a good balance between the airflow rate, air temperature rise, collector efficiency and pressure loss is the key to achieving the best collector performance.

Acknowledgements

We gratefully acknowledge the financial support by the Swedish International Development Co-operation Agency (Sida) for this study in the framework of the project ''Renewable Energy Technologies in Asia—A Regional Research and Dissemination Programme''. We also thank

the three anonymous reviewers for their helpful comments on a previous version of this paper.

References

Arulanandam, S.J., Hollands, K.G.T., Brundrett, E., 1999. A CFD heat transfer analysis of the transpired solar collector under no-wind conditions. Solar Energy 67 (1–3), 93–100.

Berger, Buriot, Garnier, 1984. About the equivalent radiative temperature for clear skies. Solar Energy 32 (5).

Bi, Y., Guo, T., Zhang, L., Chen, L., 2004. Solar and ground source heat-pump system. Applied Energy 78 (2), 231–245.

Bliss, R.W., 1961. Atmospheric radiation near the surface of the ground. Solar Energy 5 (103).

Cao, S., Hollands, K.G.T., Brundrett, E., 1993. Heat exchange effectiveness of unglazed transpired-plate solar collector in 2D flow. In: Proceedings of ISES Solar World Congress 1993, Budapest, Hungary, Vol. 5, pp. 351–366.

Cengel, Y.A., Turner, R.H., 2001. Fundamentals of Thermal-Fluid Sciences. McGraw-Hill Higher Education, 2001.

Christensen, Craig., 1998. Federal Energy Management Program: Transpired Collectors (Solar Preheaters for Outdoor Ventilation Air). Available from: <http://www.eere.energy.gov/femp/pdfs/FTA_trans_coll.pdf>. Accessed in January, 2006.

Dymond, C., Kutscher, C.F., 1997. Development of a flow distribution and design model for transpired solar collectors. Solar Energy 60 (5).

Gawlik, K.M., 1995. A numerical and experimental investigation of heat transfer in the practical utilization of unglazed, transpired solar air heaters. Ph.D. Dissertation, University of Colorado, Department of Civil, Environmental, and Architectural Engineering.

Gawlik, K.M., Kutscher, C.F., 2002. Numerical and experimental investigation of low-conductivity unglazed transpired solar air heaters. In: Pearson, J.B., Farhi, B.N., (Eds.), Solar Engineering 2002: Proceedings of the International Solar Energy Conference. NREL Report No. 31708, ASME, Reno, Nevada, New York, pp. 47–55.

Gawlik, K., Christensen, C., Kutscher, C., 2005. A numerical investigation of low-conductivity unglazed, transpired solar air heaters. Journal of Solar Energy Engineering 127, 153–155.

Golneshan, A.A., Hollands, K.G.T., 1998. Experiments on forced convection heat transfer from slotted transpired plates. In: Proceedings of CSME Forum 1998, Toronto, Canada, vol. 1. Canadian Society for Mechanical Engineering, Hamilton, Canada, pp. 78–88.

GPEKS, 2006. GPEKS Construction Inc. Available from: <www.gpeks.com/solarwall/CropDrying/dry.htm>. Accessed January, 2006.

GSFC, 2006. The Warm Earth—Thermal Remote Sensing. In: Remote Sensing Tutorial. NASA/Goddard Space Flight Center, USA. Available from: <http://rst.gsfc.nasa.gov/Front/tofc.html>. Accessed in February, 2006.

Gunnewiek, L.H., Brundrett, E., Hollands, G.T., 1996. Flow distribution in unglazed transpired plate solar air heaters of large area. Solar Energy 58 (4-6), 227–237.

Hollands, K.G.T., 1998. Principles of the Transpired-plate air heating collector: the SOLARWALL, renewable energy technologies in cold climates. In: Annual Meeting of the Solar Energy Society of Canada Inc. SESCI, Ottawa, pp. 139–144.

Hollick, J.C., 1999. In: Commercial scale solar drying. Renewable Energy, 16. Pergamon Press, pp. 714–719.

IEA, 1999. Low Cost, High performance solar air-heating systems using perforated absorbers. In: IEA Solar Heating and Cooling Report No. SHC.T14.Air.I. Final Report of Task 14 Air Systems Working Group. p. 110.

Kokko, J.P., Marshal, S., 1992. Performance of the next generation of Solarwalls. In: Proceedings of the Annual Conference of the Solar Energy Society of Canada, Edmonton, Canada, July 4–8.

Kutscher, C.F., 1992. An Investigation of Heat Transfer for Air Flow through Low Porosity Perforated Plates. Ph.D. dissertation, University of Colorado, Department of Mechanical Engineering.

Kutscher, C.F., 1994. Heat exchanger effectiveness and pressure drop for air flow through perforated plates, with and without crosswind. ASME Journal of Heat Transfer 116, 391–399.

Kutscher, C.F., 1997. Transpired solar collector systems: a major advance in solar heating. Energy Business Technology Sourcebook. In: Proceedings of the 19th World Energy Engineering Congress, NREL Report No. 24373, November 6–8, 1996, Atlanta, Georgia, Chapter 61. pp. 481–489.

Kutscher, C.F., Christensen, C., Barker, G., 1991. Unglazed transpired solar collectors: an analytic model and test results. In: Proceedings of ISES Solar World Congress 1991, Elsevier Science, Vol. 2:1. pp. 1245–1250.

Kutscher, C.F., Christensen, C., Barker, G., 1993. Unglazed transpired solar collectors: heat loss theory. ASME Journal of Solar Engineering 115 (3), 182–188.

Kutscher, C., Christensen, C., Gawlik, K., 2003. Letter to the Editor (in response to wind heat loss paper by Fleck et al.). Solar Energy 74, 353–354.

Löf, George O.G., 1981. Air-based solar systems for space heating. In: Kreider, J.F., Kreith, F. (Eds.), Solar Energy Handbook. McGraw-Hill, New York.

Martin, M., Berdahl, P., 1984. Characteristics of infrared sky radiation in the United States. Solar Energy 33 (3–4), 321–336.

Pangavhane, D.R., Sawhney, R.L., Sarsavadia, P.N., 2002. Design, development and performance testing of a new natural convection dryer. Energy 27, 579–590.

Pesaran, A.A., Wipke, K., 1994. Use of unglazed transpired solar collectors for desiccant cooling. Solar Energy Journal 52 (5), 1994.

Signorelli, S., Kohl, T., 2004. Regional ground surface temperature mapping from meteorological data. Global and Planetary Change 40, 267–284.

SOLARWALL, 2001, 2006. The SOLARWALL Solar Heating System. Conserval Engineering Inc., Canada. Available from: <http://www.solarwall.com/>. Accessed in November, 2001 and January, 2006.

Summers David, N., 1996. Thermal Simulation and Economic Assessment of Unglazed Transpired Collector System. Wisconsin Energy Bureau, University of Wisconsin, USA.

Swinbank, W.C., 1963. Long-wave radiation from clear skies. Quarterly Journal of Royal Meteorological Society 89, 339–348.

Van Decker, G.W.E., Hollands, K.G.T., Brunger, A.P., 1996. Heat exchange effectiveness of unglazed transpired-plate solar collector in 3D flow. In: Goietzburger, A., Luther, J. (Eds.), Proceedings of EuroSun 96, Freiburg, Germany. DGS–Sonnen energie Verlags GmbH, Munchen, Germany, pp. 130–846.

Van Decker, G.W.E., Hollands, K.G.T., 1999. An empirical heat transfer equation for the transpired solar collectors, including no-wind conditions. In: Proceedings of the ISES 99 Solar World Congress, Australia.

Van Decker, G.W.E., Hollands, K.G.T., Brunger, A.P., 2001. Heat exchange relations for unglazed transpired solar collectors with circular holes on a square or triangular pitch. Solar Energy 71 (1), 33–45.